Available online at www.sciencedirect.com
ScienceDirect
Journal of Power Sources 168 (2007) 469–476
JOURNAL OF POWER SOURCES
www.elsevier.com/locate/jpowsour

Parallel operation characteristics of PEM fuel cell and microturbine power plants

M. Uzunoglu [a,b], O. Onar [a,b], M.Y. El-Sharkh [a,*], N.S. Sisworahardjo [a], A. Rahman [a], M.S. Alam [a]

[a] *Department of Electrical and Computer Engineering, University of South Alabama, Mobile, AL 36688, USA*
[b] *Yildiz Technical University, Istanbul 34349, Turkey*

Received 8 February 2007; received in revised form 12 March 2007; accepted 13 March 2007
Available online 18 March 2007

Abstract

This paper reports on the dynamic behavior of a 250 kW proton exchange membrane fuel cell power plant (PEM FCPP) and a 250 kW microturbine (MT) when operating in parallel. A load sharing control scheme is used to distribute the load equally between the PEM FCPP and the MT. For stand alone operation of a PEM FCPP, a set of batteries or ultracapacitors are needed in order to satisfy the power mismatch during transient periods. Using MT in parallel with the PEM FCPP helps in eliminating the need for storage devices. Models for the PEM FCPP and the MT with power, voltage and speed controls are used to determine the dynamic response of the system to a step change in the load. Simulation results indicate viability of parallel operation of the PEM FCPP and the MT. These results are obtained using MATLAB®, Simulink®, and SimPowerSystems®.
© 2007 Elsevier B.V. All rights reserved.

Keywords: Distributed generation; Dynamic model; Microturbine; Parallel operation; Proton exchange membrane fuel cell; Simulation

1. Introduction

Due to strict power quality and system reliability requirements, new approaches for power generation and transmission have evolved. One of these is the microgrid. Microgrids are low power generators clustered to supply residential and/or commercial loads. The primary advantage of the microgrid is the elimination of the cost and minimization of transmission system problems, since generators are built close to load centers. Also, the purchase and sale of energy is possible if the microgrid system is grid connected. Fuel cells and microturbines are among the potential candidates that are suitable for supplying electric and thermal energy in microgrid system.

Fuel cells are not only characterized by higher efficiency than conventional power plants, but they are also environmentally clean, have extremely low emission of oxides of nitrogen and sulfur and have very low noise. The components of the fuel cell system include the fuel processing unit or the reformer, the fuel cell stack, and the power conditioning unit [1,2]. The reformer produces hydrogen to supply the fuel cell stack by processing any hydrocarbon fuel such as propane, methane, or methanol. Using the hydrogen supply and oxygen from the air, the fuel cell stack produces electricity and water through an electrochemical process. The output from the fuel cell is dc power. To provide power to a residential load, or to the electrical grid, a power conditioning unit is needed. Many models have been proposed to simulate the fuel cell in the literature [3–7]. Due to the low working temperature (80–100 °C) and fast start up, proton exchange membrane (PEM) fuel cell power plants (FCPPs) are the best candidate for residential and commercial applications. Based on the model introduced in [3,4], a model for a 250 kW PEM FCPP is developed and used to study the dynamic behavior in response to a step change.

Microturbines (MT) are small and simple gas turbines that have three main components: compressor, combustor, and turbine. The high pressure air from the compressor when mixed with the injected fuel forms a combustible mixture. The mixture is ignited in the combustor to produce hot gas flow, which is used to drive the turbine [8]. Two distinct types of MT are identified in the literature, the single- and split-shaft MT [9].

* Corresponding author. Tel.: +1 251 461 1562; fax: +1 251 460 6028.
E-mail addresses: muzunoglu@usouthal.edu (M. Uzunoglu), onar@usouthal.edu (O. Onar), yel-shark@usouthal.edu (M.Y. El-Sharkh), nurh@ieee.org (N.S. Sisworahardjo), arahman@usouthal.edu (A. Rahman), malam@usouthal.edu (M.S. Alam).

0378-7753/$ – see front matter © 2007 Elsevier B.V. All rights reserved.
doi:10.1016/j.jpowsour.2007.03.038

Single-shaft MT is high speed in nature, where the electric generator and turbine are mounted on the same shaft. Split-shaft MT uses a gearbox to connect the electric generator to the turbine shaft. Many models are used in the literature to describe the behavior of the MT [9–13]. In this paper, the model used in [10] has been modified by adding speed and voltage control loops.

This study uses a 250 kW PEM FCPP connected in parallel with a 250 kW MT to supply power to a common load. The paper focuses on the dynamic response of the system and the individual generators to a sharp increase and decrease in the load.

The paper is organized as follows: Section 2 presents the configuration of the proposed system. In Section 3, a modified 250 kW PEM FCPP model is introduced. Section 4 presents the MT model. Tests and results are discussed in Section 5 followed by the conclusion in Section 6.

2. Parallel operation of PEM FCPP and MT

Fig. 1 shows the connection of the MT and PEM FCPP in parallel. Many different configurations can be visualized based on the technology related to the MT and the PEM FCPP. In the proposed system, a synchronous generator (SG) is coupled to the MT shaft. Since the SG produces 660 V, a transformer is used to step down the voltage to 440 V to match the PEM FCPP voltage. The PEM FCPP produces a dc voltage of 440 V. A dc/dc converter with a gain of 1.5 is used to boost the dc voltage. A dc/ac inverter is used to convert the dc voltage to an ac voltage of 440 V. The SG and PEM FCPP ac voltages are controlled by controlling the field excitation and modulation index, respectively. The MT and the PEM FCPP are connected in parallel at the ac bus to supply a common load. Details of the MT and the PEM FCPP models and controls are given in subsequent sections.

For parallel operation of the MT and PEM FCPP, a load sharing control is needed (Fig. 1). The load sharing control strategy as shown in Fig. 1 can be summarized as follows:

- During steady-state conditions, the MT and the PEM FCPP share the load equally.
- Due to the slower response of the PEM FCPP during transient periods, the MT compensates for the power mismatch until the PEM FCPP is able to supply its share of the load.

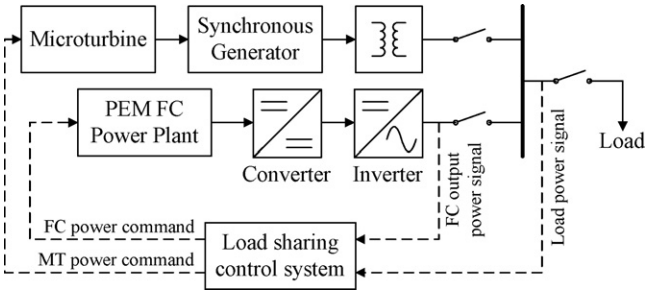

Fig. 1. Parallel operation of PEM FCPP and MT system.

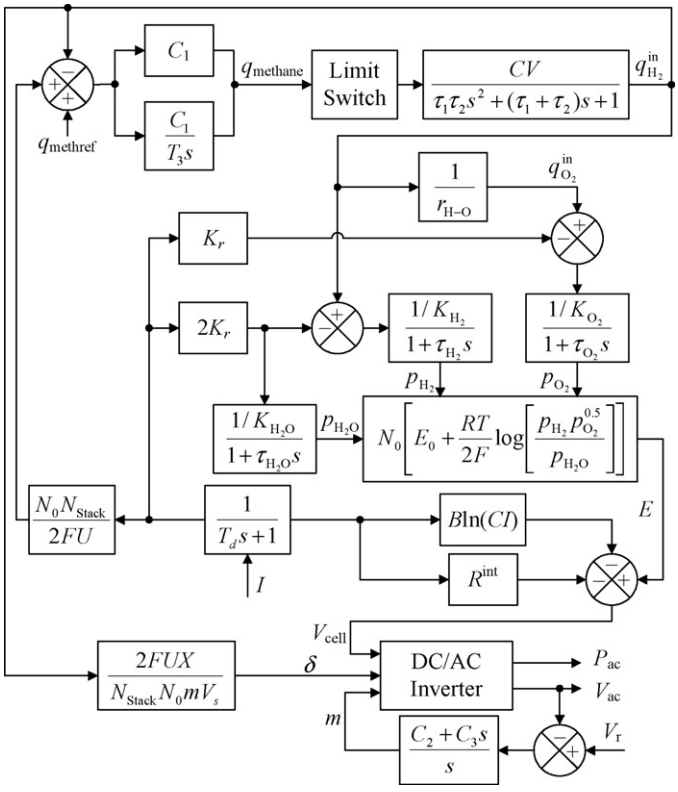

Fig. 2. PEM FCPP system block diagram.

3. PEM fuel cell model

3.1. Model description

In [3,4,14] a model of a PEM FCPP is introduced. In this paper the model has been modified to simulate a 250 kW PEM fuel cell.

The model is based on simulating the relationship between the output voltage and partial pressures of hydrogen, oxygen, and water. The detailed model shown in Fig. 2 [3,4,14] includes reformer and power conditioning unit.

The 250 kW PEM FCPP model parameters are based on a 440 V dc bus voltage with a stack current capacity of 94 A, and a cell voltage of 0.8 V. Based on the above figures, the PEM FCPP consists of six parallel stacks, each stack has 550 cells in series. Using the indicated number of cells and stacks the 250 kW PEM FCPP model parameters are given in Table 1.

3.2. FCPP power control

Power control scheme has been developed in [14] that can be summarized as follows:

$$P_{ac} = \frac{m V_{cell} V_s}{X} \sin(\delta) \quad (1)$$

where P_{ac} is the ac power, m the modulation index, V_{cell} the dc voltage, V_s the load voltage, X the external line reactance, and δ is the phase angle of the ac voltage mV_{cell}.

Table 1
PEM FCPP model parameters

Parameter	Value
Stack temperature	343 K
Faraday's constant (F)	96,484,600 C kmol^{-1}
Universal gas constant (R)	8314.47 J (kmol K)$^{-1}$
No load cell voltage (E_0)	0.8 V
Number of cells per stack (N_0)	550
Number of stacks (N_{stack})	6
K_r constant = $N_0/(4F)$	1.4251×10^{-6} kmol (s A)$^{-1}$
Utilization factor (U)	0.8
Hydrogen valve constant (K_{H_2})	4.22×10^{-5} kmol (s atm)$^{-1}$
Water valve constant (K_{H_2O})	7.716×10^{-6} kmol (s atm)$^{-1}$
Oxygen valve constant (K_{O_2})	2.11×10^{-5} kmol (s atm)$^{-1}$
Hydrogen time constant (τ_{H_2})	3.37 s
Water time constant (τ_{H_2O})	18.418 s
Oxygen time constant (τ_{O_2})	6.74 s
Reformer time constant (τ_1)	2 s
Reformer time constant (τ_2)	2 s
Reformer PI gain (C_1)	0.25
Conversion factor (CV)	2
Activation voltage constant (B)	0.04777 A^{-1}
Activation voltage constant (C)	0.0136 V
Internal resistance (R^{int})	0.2778 Ω
External line reactance (X)	0.05 Ω
PI gain constants C_2, C_3	0.1, 10
Voltage reference signal (V_r)	1.0 p.u.
Methane reference signal ($Q_{methref}$)	0.000015 kmol s^{-1}
Hydrogen–oxygen flow ratio (r_{H-O})	1.168
Current delay time constant (T_d)	3 s

Assuming a lossless inverter:

$$P_{ac} = P_{dc} = V_{cell} I \tag{2}$$

$$q_{H_2} = \frac{N_{Stack} N_0 I}{2FU} \tag{3}$$

where P_{dc} is the dc power, I the stack current, q_{H_2} the input molar flow of hydrogen, N_{Stack} the number of stacks, N_0 the number of cells per stack, F the Faraday's constant, and U is the utilization factor.

From (1)–(3):

$$\sin(\delta) = \frac{2FUX}{m V_s N_0 N_{Stack}} q_{H_2}. \tag{4}$$

Assuming a small phase angle $\sin(\delta) \cong \delta$,

$$\delta = \frac{2FUX}{m V_s N_0 N_{Stack}} q_{H_2}. \tag{5}$$

Eq. (5) describes the relationship between output voltage phase angle δ and hydrogen flow q_{H_2}. Eqs. (1) and (5) show that the active power as a function of the voltage phase angle δ can be controlled using the amount of hydrogen flow.

Output voltage can be controlled by the modulation index m. The modulation index is controlled using a PI controller. The input to the PI controller is the error signal (difference between the ac terminal voltage V_{ac} and reference voltage V_r).

4. Microturbine model

4.1. Model description

As mentioned earlier, microturbines are classified in two categories, the single-shaft or high speed turbine and split-shaft or low speed turbine. In the single-shaft configuration, the compressor, turbine, and electric generator are mounted on the same shaft. The turbine speed is in the range of 50,000–120,000 rpm. The frequency of the produced voltage is in the range of 1500–4000 Hz. To reduce the frequency to 60 Hz, a cyclo-converter is used. In split-shaft microturbine, the electric generator is driven through a gearbox. The gearbox is used to reduce the speed to 3600 rpm. Assuming a two-pole synchronous generator (SG), the frequency will be 60 Hz. In this case, no power electronic devices are needed for frequency conversion.

In this paper, a split-shaft model is used to determine the dynamic behavior of a microturbine. In [10], the authors used the GAST model without speed control to simulate the split-shaft microturbine. The GAST model, which is developed by general electric (GE), is one of the most commonly used model to simulate gas turbines. In this paper, due to the use of a SG, a speed controller is developed and used with the GAST model. The model details and parameters are shown in Fig. 3 and Table 2, respectively.

4.2. Simplified synchronous generator model

A simplified model of a synchronous generator is given in [15]. A modified version of this model is presented in Fig. 4.

The equations that are used to drive the synchronous machine model are explained in Appendix A. To simulate the synchronous machine, the authors used a predefined model existed in SimPowerSystems of the MATLAB software [16]. The model parameters are as shown in Table 3.

4.3. MT speed control

As shown in Fig. 3, speed control is achieved by comparing the rotor speed ω_r with a reference speed ω_{ref}. A PI controller

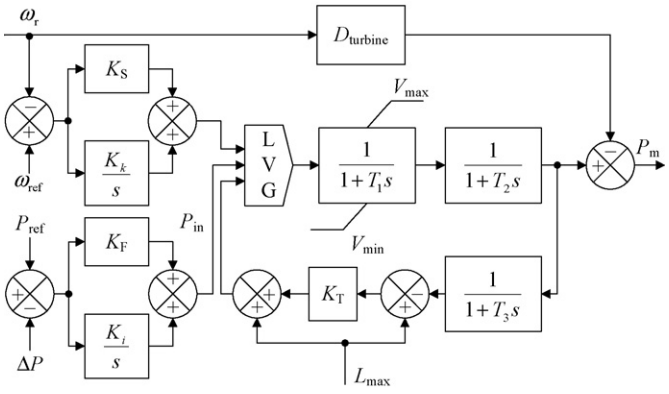

Fig. 3. MT system block diagram with speed and power control.

Table 2
MT model parameters

Parameter	Value
Rated power ($P_{\text{rated-MT}}$)	250 kW
Real power reference (P_{ref})	1.0 p.u.
Turbine damping (D_{turbine})	0.03
Fuel system lag time constant (T_1)	10.0 s
Fuel system lag time constant (T_2)	0.1 s
Load limit time constant (T_3)	3.0 s
Load limit ($L_{\max}$)	1.2
Maximum value position ($V_{\max}$)	1.2
Minimum value position ($V_{\min}$)	–0.1
Temperature control loop gain (K_{T})	1.0
Power control proportional gain (K_{F})	0.1
Power control integral gain (K_i)	1.0
Speed control proportional gain (K_{S})	1000
Speed control integral gain (K_k)	12.5
Speed reference (ω_{ref})	1.0 p.u.

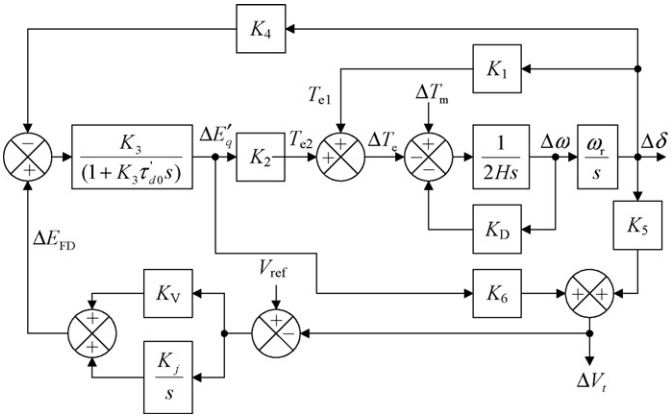

Fig. 4. Synchronous generator block diagram with voltage control.

is used to control the error signal ($\omega_{\text{ref}} - \omega_{\text{r}}$). The PI controller output is then connected as a low value gate input.

4.4. MT real power control

Referring to Fig. 3, to control the mechanical output power from the microturbine, a PI controller is used. The input to the PI controller is the error signal ($P_{\text{ref}} - \Delta P$), where ΔP is the difference between the generated and the load power.

Table 3
Synchronous machine model parameters

Parameter	Value
Rated power ($P_{\text{rated-SG}}$)	250 kW
Rated line to line voltage (V_{rated})	660 V
Frequency (F)	60 Hz
Inertia constant (H)	0.822 s
Damping factor (K_{D})	33.63 p.u.
Number of poles (P)	2
Internal resistance (R)	0.02 p.u.
Internal reactance (X)	0.3 p.u.

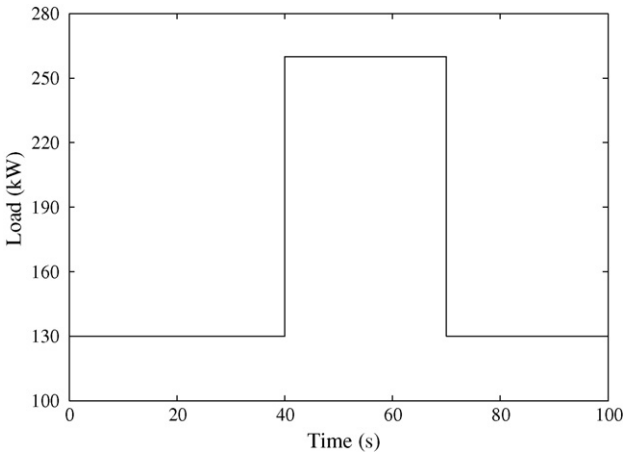

Fig. 5. Step change in load.

4.5. MT voltage control

As stated in Table 3, the SG output voltage is 660 V. To compare the SG voltage and the PEM FCPP voltage (440 V) a transformer is used to step down the SG voltage to 440 V at the load terminals. A PI controller is used to control the output voltage by controlling the excitation voltage of the synchronous generator. The input signal to the PI controller is the difference between the output voltage and reference voltage V_{ref}. The parameters for the PI controller are $K_{\text{V}} = 0.005$, and $K_j = 0.1$.

5. Test and results

To evaluate the parallel operation of the PEM FCPP and the MT system, a step change in the load is used as illustrated in Fig. 5. The simulation time is 100 s, the initial load is 130 kW, and increased to 260 kW after 40 s. After 70 s, the load is decreased to 130 kW. The effect of changing the load on the output power of the PEM FCPP and the MT are shown in Figs. 6 and 7.

As shown in Figs. 6 and 7, when the load increases the PEM FCPP is unable to supply its share instantaneously. In transient

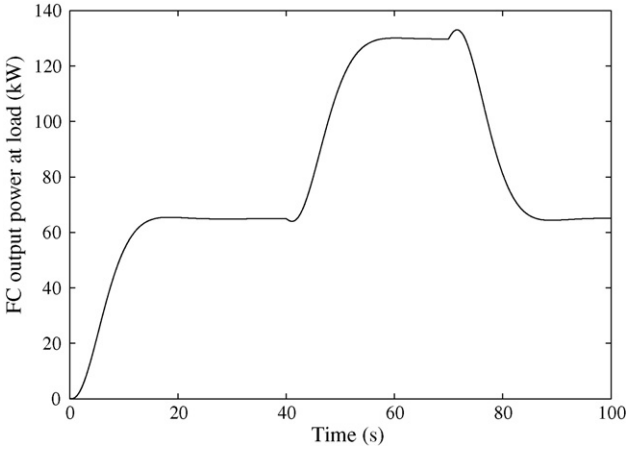

Fig. 6. PEM FCPP output power.

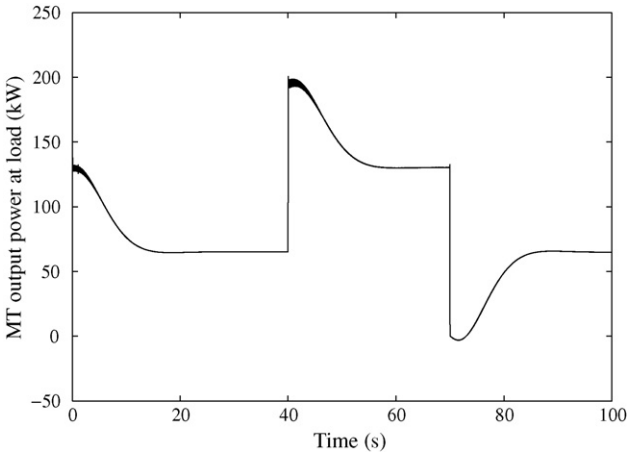

Fig. 7. MT output power.

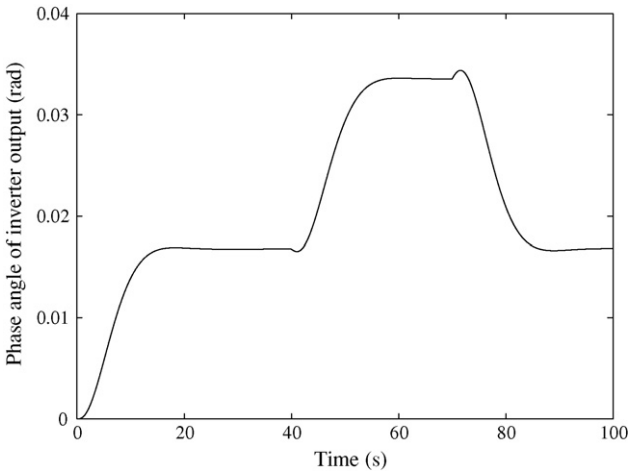

Fig. 9. Inverter phase angle.

condition such as a step-up in load demand, the microturbine is used to compensate the FCPP delay until the FCPP output power increases and matches half of the load. During the first 40 s, the system started with a load of 130 kW, initially, the MT provides a 130 kW while the FCPP output is zero. As the FCPP output power increases, the MT output power decreases. After, about 17 s, the MT and the FCPP equally share the load. The delay in the FCPP output is mainly caused by the reformer, due to the slow gas processing response, as shown from the hydrogen flow and inverter phase angle (Figs. 8 and 9). The other reason of this delay is the thermal inertia, which plays an important role in the response time of the fuel cells. In a transient condition, the temperatures of each stage of the reformer change slowly and continuously because of the high thermal inertia of the materials and the reactants. At $t = 40$ s, the load changes suddenly to 260 kW, the MT produces about 198 kW instantaneously after the load increases (Fig. 7). The MT output power deceases gradually as the PEM FCPP output increases. At time $t = 57$ s, the PEM FCPP and the MT share the load equally.

During load reduction period, $t > 70$ s, the PEM FCPP is unable to decrease the output suddenly to 65 kW. In this case, the MT output at the load terminals decreases to −0.293 kW. This means that when t is between 70 and 80 s, the PEM FCPP is supplying the load as well as the losses in the transformer and the transmission line between the SG and the load.

Despite the fact that the MT response is much faster than that of the PEM FCPP, the mechanical power output from the turbine suffers a time delay as shown in Fig. 10. During such delay periods the power mismatch is compensated by the rotor inertia, which causes a momentary decrease/increase in the rotor speed as illustrated in Fig. 11. During the low/high rotor speed periods, the speed controller and the power controller increase/decrease the input power to the turbine. When the mechanical input power matches the electrical power output, the speed controller brings the rotor speed back to synchronous value (Fig. 11). As indicated in Fig. 12, the summation of the output power from the PEM FCPP and the MT matches the step change in load as given in Fig. 5.

The change of the ac voltage of the PEM FCPP is insignificant (Fig. 13). This is mainly due to the effectiveness of the PEM FCPP voltage controller as shown in Fig. 2. Fig. 14 shows the change of fuel cell stack dc voltage due to load changes.

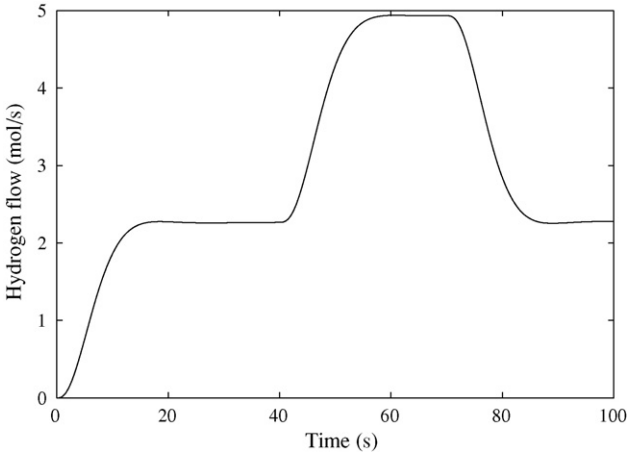

Fig. 8. Hydrogen flow in PEM FCPP.

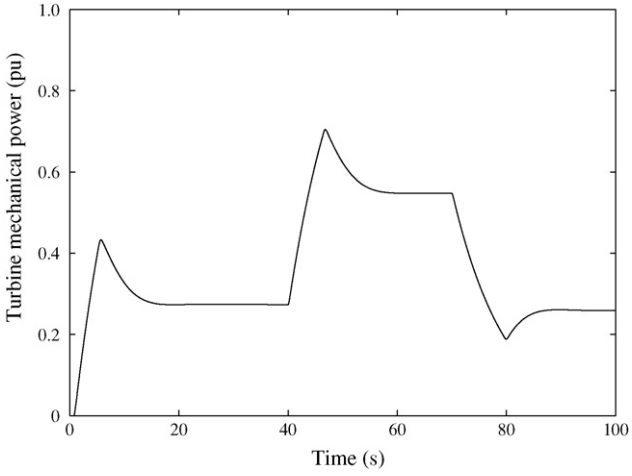

Fig. 10. Turbine mechanical power.

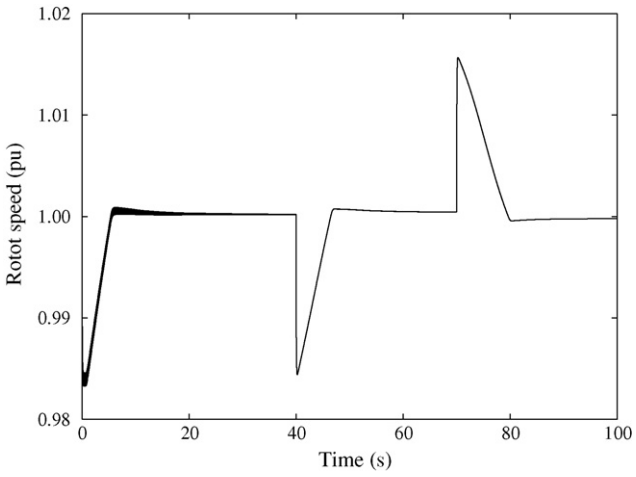

Fig. 11. Synchronous generator rotor speed.

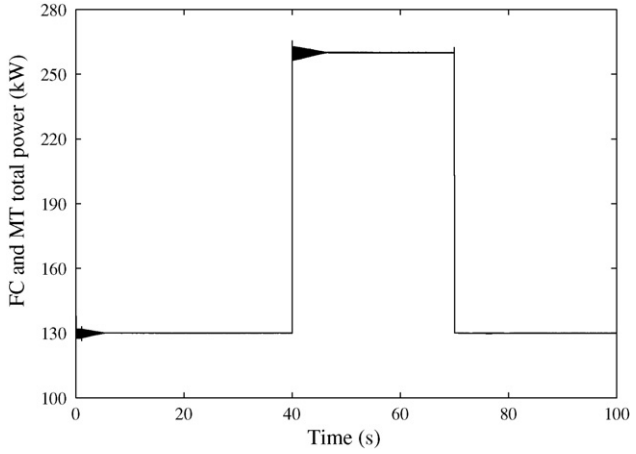

Fig. 12. Total output power from the PEM FCPP and the MT.

In order to produce a constant ac voltage, the modulation index changes with inverse proportionality with respect to the dc voltage (Fig. 15).

During load changes, the MT voltage is experiencing a short period of oscillation as illustrated in Fig. 16. As a result of the voltage oscillations and load changes, the voltage controller changes the excitation level to keep the output voltage constant at 660 V. Fig. 17 shows the changes in the excitation voltage.

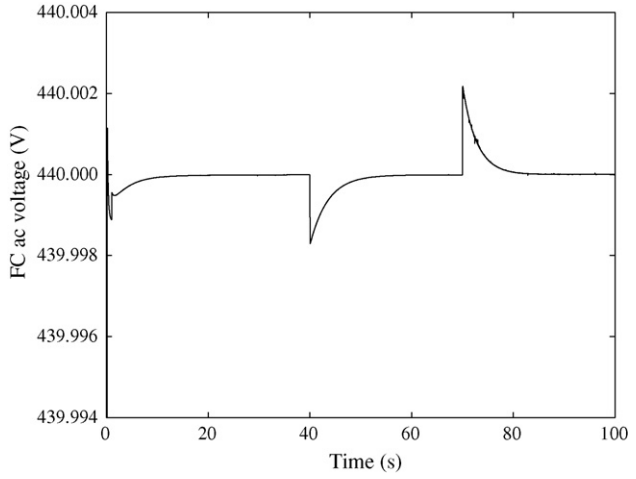

Fig. 13. PEM FCPP ac voltage.

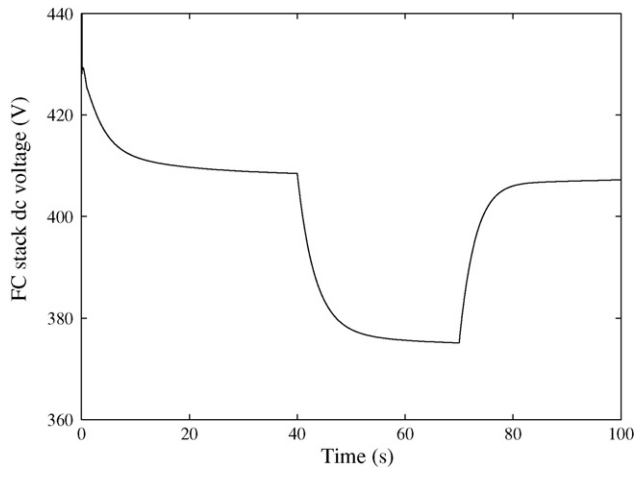

Fig. 14. PEM FCPP stack output voltage.

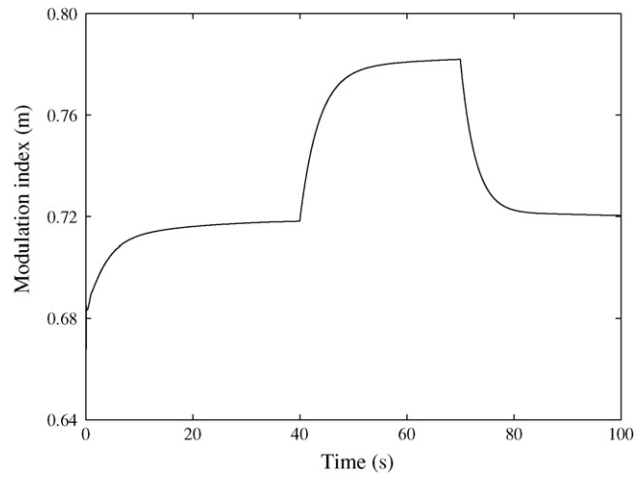

Fig. 15. Inverter modulation index.

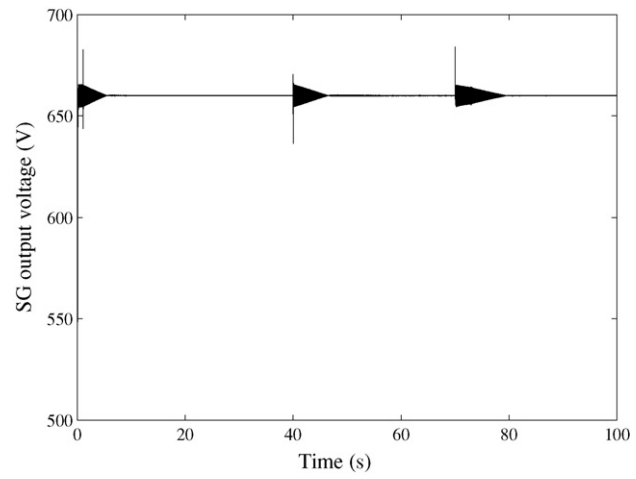

Fig. 16. MT voltage.

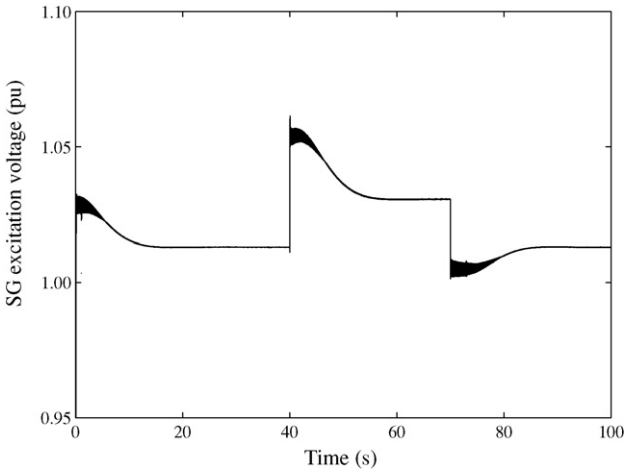

Fig. 17. SG excitation voltage.

6. Conclusion

Dynamic plots reflecting the parallel operation of PEM FCPP and MT are evaluated. Dynamic models of the 250 kW PEM FCPP and MT with speed and power control are developed. The step load change test results indicate that the proposed system configuration is able to accommodate drastic changes in the load. In stand alone operation of the PEM FCPP, a set of batteries or ultracapacitors are essential in order to satisfy the power mismatch during the transient period. Using the MT in parallel with the PEM FCPP can help in eliminating the need for storage devices. Although the MT response has a better load following capability, the mechanical power output experiences a momentary delay. During this delay period, rotor speed decreases/increases as part of the rotor kinetic energy is used to compensate the power mismatch. By the time the MT system reaches a new equilibrium point, the speed controller brings the rotor speed back to synchronous speed. To generalize the fact that the MT can be used to preclude the storage devices in FCPP, more simulation for different situations and different control scenarios may be used.

Acknowledgement

This work was supported in part by the U.S. Department of Energy under Grant DE-FG02-05CH11295.

Appendix A

Synchronous machine model as explained in [15] is constructed based on synchronous machine swing equation. Swing equation for power system dynamics can be expressed in many forms. Given ω in electrical deg s^{-1}, swing equation is expressed as:

$$\frac{\pi H}{90}\frac{d\omega}{dt} = T_m - T_e = T_a. \quad (A.1)$$

Linearizing the swing Eq. (A.1) results in an equation as shown in (A.2).

$$\tau_j \Delta\omega s = \Delta T_m - \Delta T_e \quad (A.2)$$

The basic equations for the simplified linear synchronous generator model consist of three equations, i.e.,

$$\Delta E'_q = \frac{K_3}{1 + K_3\tau'_{d0}s}\Delta E_{FD} - \frac{K_3K_4}{1 + K_3\tau'_{d0}s}\Delta\delta \quad (A.3)$$

$$\Delta T_e = K_1\Delta\delta + K_2\Delta E'_q \quad (A.4)$$

$$\Delta V_t = K_5\Delta\delta + K_6\Delta E'_q. \quad (A.5)$$

The constants K_1, K_2, K_3, K_4, K_5, and K_6 are dependent upon the network parameters, the quiescent operating conditions, and the infinite bus voltage.

The simplified synchronous generation model as presented in Fig. 3 is obtained by combining the effect of the damping torque with voltage control, and Eqs. (A.2)–(A.5). The variables are defined as follows:

T_m	mechanical torque
T_a	accelerating torque
T_e	electromagnetic torque
τ_j	time constant ($\tau_j = 2H/\omega_r$)
τ'_{d0}	*d*-axis transient open circuit time constant
δ	rotor angle
V_t	terminal voltage
E'_q	rms of the peak stator voltage
E_{FD}	stator EMF
ω_r	rotor angular speed
K_1	change in the electrical torque for small change in rotor angle at constant *d*-axis flux linkage
K_2	change in the electrical torque for small change in the *d*-axis flux linkage at constant rotor angle
K_3	impedance factor
K_4	constant related to demagnetizing effect
K_5	change in the terminal voltage V_t for a small change in rotor angle at constant *d*-axis flux linkage
K_6	change in the terminal voltage V_t for a small change in the *d*-axis flux linkage at constant rotor angle
K_D	damping constant
H	inertia constant

References

[1] J.E. Larmine, A. Dicks, Fuel Cell Systems Explained, second ed., John Wiley and Sons, 2000.
[2] W. Vielstich, A. Lamm, H. Gasteiger, Handbook of Fuel Cells: Fundamentals, Technology, Applications, 4-volume set, John Wiley and Sons, 2003.
[3] M.Y. El-Sharkh, A. Rahman, M.S. Alam, P.C. Byrne, A.A. Sakla, T. Thomas, J. Power Sources 138 (1/2) (2004) 199–200.
[4] M. Uzunoglu, M.S. Alam, IEEE Trans. Energy Conver. 21 (3) (2006) 767–775.
[5] J.C. Amphlett, R.F. Mann, B.A. Peppley, P.R. Roberge, A. Rodrigues, J. Power Sources 61 (1996) 183–188.
[6] J. Padulles, G.W. Ault, J.R. McDonald, J. Power Sources 86 (2000) 495–500.

[7] J.C. Amphlett, R.M. Baumert, R.F. Mann, B.A. Peppley, P.R. Roberge, A. Rodrigues, J. Power Sources 49 (1994) 349–356.
[8] W.I. Rowen, Trans. ASME 105 (1) (1983) 865–869.
[9] G.N. Kariniotakis, N.L. Soultanis, A.I. Tsouchnikas, S.A. Papathanasiou, N.D. Hatziargyriou, Proceedings of Future Power Systems Conference, Amsterdam, 2005, pp. 1–7.
[10] Y. Zhu, K. Tomsovic, Electr. Power Syst. Res. 62 (1) (2002) 1–11.
[11] F. Jurado, Energy Convers. Manage. 46 (3) (2005) 385–401.
[12] M. Nagpal, A. Moshref, G.K. Morison, P. Kundur, Proceedings of the IEEE/PES 2001 Winter Meeting, Columbus, Ohio, USA, January/February, 2001, pp. 652–656.
[13] S.R. Guda, Modeling and power management of a hybrid wind microturbine power generation system, M.S. Thesis, Department Electrical Eng., Montana State University, Bozeman, Montana.
[14] M.Y. El-Sharkh, A. Rahman, M.S. Alam, P.C. Byrne, A.A. Sakla, T. Thomas, IEEE Trans. Power Syst. 19 (4) (2004) 2022–2028.
[15] P.M. Anderson, A.A. Fouad, Power System Control and Stability, vol. 1, The Iowa State University Press, 1977.
[16] SimPowerSystems User's Guide, Version 4, The MathWorks Inc. 2006.